

Performance analysis of experimentally viable photonic crystal enhanced thermophotovoltaic systems

Yi Xiang Yeng,^{1,2,*} Walker R. Chan,^{1,2} Veronika Rinnerbauer,¹
John D. Joannopoulos,^{1,2,3,4} Marin Soljačić,^{1,2,3,4} and Ivan Celanovic²

¹Research Laboratory of Electronics, Massachusetts Institute of Technology,
Cambridge, Massachusetts 02139, USA

²Institute of Soldier Nanotechnologies, Massachusetts Institute of Technology,
Cambridge, Massachusetts 02139, USA

³Department of Physics, Massachusetts Institute of Technology,
Cambridge, Massachusetts 02139, USA

⁴Centre for Materials Science and Engineering, Massachusetts Institute of Technology,
Cambridge, Massachusetts 02139, USA

[*xyyeng@mit.edu](mailto:xyyeng@mit.edu)

Abstract: One of the keys towards high efficiency thermophotovoltaic (TPV) energy conversion systems lies in spectral control. Here, we present detailed performance predictions of realistic TPV systems incorporating experimentally demonstrated advanced spectral control components. Compared to the blackbody emitter, the optimized two-dimensional (2D) tantalum (Ta) photonic crystal (PhC) selective emitter enables up to 100% improvement in system efficiency. When combined with the well characterized cold side tandem filter and the latest InGaAs TPV cells, a TPV energy conversion system with radiant heat-to-electricity efficiency of 25% and power density of 0.68 W cm^{-2} is achievable today even at a relatively low temperature of 1320 K. The efficiency could be increased to $\sim 40\%$ (the theoretical 0.62 eV single bandgap TPV thermodynamic limit at 1320 K is 55%) as future implementation of more optimized TPV cells approach their theoretical thermodynamic limit.

© 2013 Optical Society of America

OCIS codes: (260.2160) Energy transfer; (050.5298) Photonic crystals; (290.6815) Thermal emission.

References and links

1. C. A. Wang, H. K. Choi, S. L. Ransom, G. W. Charache, L. R. Danielson, and D. M. Depoy, "High-quantum-efficiency 0.5 eV GaInAsSb/GaSb thermophotovoltaic devices," *Appl. Phys. Lett.* **75**, 1305–1307 (1999).
2. O. V. Sulima and A. W. Bett, "Fabrication and simulation of GaSb thermophotovoltaic cells," *Sol. Ener. Mater. Sol. Cells* **66**, 533–540 (2001).
3. R. R. Siergiej, B. Wernsman, S. A. Derry, R. G. Mahorter, R. J. Wehrer, S. D. Link, M. N. Palmisiano, R. L. Messham, S. Murray, C. S. Murray, F. Newman, J. Hills, and D. Taylor, "20% efficient InGaAs/InPAs TPV cells," in *AIP Conference Proceedings: Thermophotovoltaic Generation of Electricity 5th Conference* (AIP, 2003), pp. 414–423.
4. M. W. Dashiell, J. F. Beausang, H. Ehsani, G. J. Nichols, D. M. Depoy, L. R. Danielson, P. Talamo, K. D. Rahner, E. J. Brown, S. R. Burger, P. M. Fourspring, W. F. Topper Jr., P. F. Baldasaro, C. A. Wang, R. K. Huang, M. K. Connors, G. W. Turner, Z. A. Shellenbarger, G. Taylor, J. Li, R. Martinelli, D. Donetski, S. Anikeev, G. L. Belenky, and S. Luryi, "Quaternary InGaAsSb thermophotovoltaic diodes," *IEEE Trans. Electron. Dev.* **53**, 2879–2891 (2006).

5. H. H. Kolm, "Solar-battery Power Source," Tech. Rep., MIT Lincoln Laboratory. Quarterly Progress Report, Group 35, pp. 13 (1956).
6. B. D. Wedlockt, "Thermo-photo-voltaic energy conversion," Proc. IEEE **51**, 694–698 (1963).
7. T. J. Coutts, "A review of progress in thermophotovoltaic generation of electricity," Renew. Sust. Energ. Rev. **3**, 77–184 (1999).
8. M. Zenker, A. Heinzl, G. Stollwerck, J. Ferber, and J. Luther, "Efficiency and power density potential of combustion-driven thermophotovoltaic systems using GaSb photovoltaic cells," IEEE Trans. Electron. Dev. **48**, 367–376 (2001).
9. B. Wernsman, R. G. Mahorter, R. R. Siergiej, S. D. Link, R. J. Wehrer, S. J. Belanger, P. M. Fourspring, S. Murray, F. Newman, D. Taylor, and T. Rahmlow, "Advanced thermophotovoltaic devices for space nuclear power systems," in *AIP Conference Proceedings: Space Technology and Applications International Forum* (AIP, 2005), pp. 1441–1448.
10. R. W. Kaszeta, Y. X. Yeng, M. Ghebrehirhan, J. D. Joannopoulos, M. Soljačić, and I. Celanovic, "Advanced radiative emitters for radioisotope thermophotovoltaic power systems," in *5th World Conference on Photovoltaic Energy Conversion / Ninth Thermophotovoltaic World Conference* (2010).
11. N. P. Harder and P. Wurfel, "Theoretical limits of thermophotovoltaic solar energy conversion," Semicond. Sci. Technol. **18**, S151–S157 (2003).
12. V. M. Andreev, A. S. Vlasov, V. P. Khvostikov, O. A. Khvostikova, P. Y. Gazaryan, S. V. Sorokina, and N. A. Sadchikov, "Solar thermophotovoltaic converters based on tungsten emitters," J. Sol. Ener. Eng. **129**, 298–303 (2007).
13. C. S. Murray, C. J. Crowley, S. Murray, N. A. Elkouh, R. W. Hill, and D. E. Chubb, "Thermophotovoltaic converter design for radioisotope power systems," in *AIP Conference Proceedings: Thermophotovoltaic Generation of Electricity 6th Conference* (AIP, 2004), pp. 123–132.
14. R. A. Lowe, D. L. Chubb, S. C. Farmer, and B. S. Good, "Rare-earth garnet selective emitter," Appl. Phys. Lett. **64**, 3551–3553 (1994).
15. H. Yugami, H. Sai, K. Nakamura, N. Nakagawa, and H. Ohtsubo, "Solar thermophotovoltaic using $\text{Al}_2\text{O}_3/\text{Er}_3\text{Al}_5\text{O}_{12}$ eutectic composite selective emitter," in *Conference Record of the Twenty Eighth IEEE Photovoltaic Specialists Conference* (IEEE, 2000), pp. 1214–1217.
16. L. Ferguson and F. Dogan, "A highly efficient NiO-Doped MgO matched emitter for thermophotovoltaic energy conversion," Mat. Sci. Eng. B **83**, 35–41 (2001).
17. B. Bitnar, W. Durisch, J.-C. Mayor, H. Sigg, and H. Tschudi, "Characterisation of rare earth selective emitters for thermophotovoltaic applications," Sol. Ener. Mater. Sol. Cells **73**, 221–234 (2002).
18. A. Narayanaswamy and G. Chen, "Thermal emission control with one-dimensional metallodielectric photonic crystals," Phys. Rev. B **70**, 125101 (2004).
19. D. L. C. Chan, M. Soljačić, and J. D. Joannopoulos, "Thermal emission and design in one-dimensional periodic metallic photonic crystal slabs," Phys. Rev. E **74**, 016609 (2006).
20. A. Heinzl, V. Boerner, A. Gombert, B. Bläsi, V. Wittwer, and J. Luther, "Radiation filters and emitters for the NIR based on periodically structured metal surfaces," J. Mod. Opt. **47**, 2399–2419 (2000).
21. M. U. Pralle, N. Moelders, M. P. McNeal, I. Puscasu, A. C. Greenwald, J. T. Daly, E. A. Johnson, T. George, D. S. Choi, I. El-Kady, and R. Biswas, "Photonic crystal enhanced narrow-band infrared emitters," Appl. Phys. Lett. **81**, 4685–4687 (2002).
22. H. Sai and H. Yugami, "Thermophotovoltaic generation with selective radiators based on tungsten surface gratings," Appl. Phys. Lett. **85**, 3399–3401 (2004).
23. D. L. C. Chan, M. Soljačić, and J. D. Joannopoulos, "Thermal emission and design in 2D-periodic metallic photonic crystal slabs," Opt. Express **14**, 8785–8796 (2006).
24. I. Celanovic, N. Jovanovic, and J. Kassakian, "Two-dimensional tungsten photonic crystals as selective thermal emitters," Appl. Phys. Lett. **92**, 193101 (2008).
25. R. Biswas, D. Zhou, I. Puscasu, E. Johnson, A. Taylor, and W. Zhao, "Sharp thermal emission and absorption from conformally coated metallic photonic crystal with triangular lattice," Appl. Phys. Lett. **93**, 063307 (2008).
26. S. Y. Lin, J. Moreno, and J. G. Fleming, "Three-dimensional photonic-crystal emitter for thermal photovoltaic power generation," Appl. Phys. Lett. **83**, 380–382 (2003).
27. D. L. C. Chan, M. Soljačić, and J. D. Joannopoulos, "Direct calculation of thermal emission for three-dimensionally periodic photonic crystal slabs," Phys. Rev. E **74**, 036615 (2006).
28. T. D. Rahmlow, J. E. Lazo-wasem, E. J. Gratrix, P. M. Fourspring, and D. M. Depoy, "New performance levels for TPV front surface filters," in *AIP Conference Proceedings: Thermophotovoltaic Generation of Electricity 6th Conference* (AIP, 2004), pp. 180–188.
29. R. T. Kristensen, J. F. Beusang, and D. M. Depoy, "Frequency selective surfaces as near-infrared electromagnetic filters for thermophotovoltaic spectral control," J. Appl. Phys. **95**, 4845–4851 (2004).
30. F. O'Sullivan, I. Celanovic, N. Jovanovic, J. Kassakian, S. Akiyama, and K. Wada, "Optical characteristics of one-dimensional Si/SiO₂ photonic crystals for thermophotovoltaic applications," J. Appl. Phys. **97**, 033529 (2005).
31. T. D. Rahmlow, D. M. Depoy, P. M. Fourspring, H. Ehsani, J. E. Lazo-Wasem, and E. J. Gratrix, "Development of front surface, spectral control filters with greater temperature stability for thermophotovoltaic energy conversion,"

- in *AIP Conference Proceedings: Thermophotovoltaic Generation of Electricity 7th Conference* (AIP, 2007), pp. 59–67.
32. G. W. Charache, D. M. Depoy, P. F. Baldasaro, and B. C. Campbell, “Thermophotovoltaic devices utilizing a back surface reflector for spectral control,” *AIP Conf. Proc.* **358**, 339–350 (1996).
 33. R. K. Huang, C. A. Wang, M. K. Connors, G. W. Turner, and M. W. Dashiell, “Hybrid back surface reflector GaInAsSb thermophotovoltaic devices,” *AIP Conf. Proc.* **738**, 329–336 (2004).
 34. L. B. Karlina, M. M. Kulagina, N. K. Timoshina, A. S. Vlasov, and V. M. Andreev, “In_{0.53}Ga_{0.47}As/InP conventional and inverted thermophotovoltaic cells with back surface reflector,” *AIP Conf. Proc.* **890**, 182–189 (2007).
 35. P. F. Baldasaro, J. E. Reynolds, G. W. Charache, D. M. Depoy, C. T. Ballinger, T. Donovan, and J. M. Borrego, “Thermodynamic analysis of thermophotovoltaic efficiency and power density tradeoffs,” *J. Appl. Phys.* **89**, 3319–3327 (2001).
 36. T. A. Walsh and S. Y. Lin, “Power density and efficiency of thermophotovoltaic energy conversion using a photonic-crystal emitter and a 2-D metal-grid filter,” *IEEE Trans. Electron. Dev.* **55**, 1101–1108 (2008).
 37. P. Bermel, M. Ghebrebrhan, W. Chan, Y. X. Yeng, M. Araghchini, R. Hamam, C. H. Marton, K. F. Jensen, M. Soljačić, J. D. Joannopoulos, S. G. Johnson, and I. Celanovic, “Design and global optimization of high-efficiency thermophotovoltaic systems,” *Opt. Express* **18**, A314–A334 (2010).
 38. M. Ghebrebrhan, P. Bermel, Y. X. Yeng, J. D. Joannopoulos, M. Soljačić, and I. Celanovic, “Tailoring thermal emission via Q-matching of photonic crystal resonances,” *Phys. Rev. A* **83**, 033810 (2011).
 39. Y. X. Yeng, M. Ghebrebrhan, P. Bermel, W. R. Chan, J. Joannopoulos, M. Soljačić, and I. Celanović, “Enabling high temperature nanophotonics for energy applications,” *Proc. Natl. Acad. Sci. USA* **109**, 2280 (2011).
 40. M. Araghchini, Y. X. Yeng, N. Jovanovic, P. Bermel, L. A. Kolodziejski, M. Soljačić, I. Celanovic, and J. D. Joannopoulos, “Fabrication of two-dimensional tungsten photonic crystals for high-temperature applications,” *J. Vac. Sci. Technol. B* **29**, 061402 (2011).
 41. V. Rinnerbauer, S. Ndao, Y. X. Yeng, J. J. Senkevich, K. F. Jensen, J. D. Joannopoulos, M. Soljačić, I. Celanovic, and R. D. Geil, “Large-area fabrication of high aspect ratio tantalum photonic crystals for high-temperature selective emitters,” *J. Vac. Sci. Technol. B* **31**, 011802 (2013).
 42. V. Rinnerbauer, Y. X. Yeng, W. R. Chan, J. J. Senkevich, J. D. Joannopoulos, M. Soljačić, and I. Celanovic, “High-temperature stability and selective thermal emission of polycrystalline tantalum photonic crystals,” *Opt. Express* **21**, 11482–11491 (2013).
 43. B. Wernsman, R. R. Siergiej, S. D. Link, R. G. Mahorter, M. N. Palmisiano, R. J. Wehrer, R. W. Schultz, G. P. Schmuck, R. L. Messham, S. Murray, C. S. Murray, F. Newman, D. Taylor, D. M. Depoy, and T. Rahmlow, “Greater than 20% radiant heat conversion efficiency of a thermophotovoltaic radiator/module system using reflective spectral control,” *IEEE Trans. Electron. Dev.* **51**, 512–515 (2004).
 44. C. J. Crowley, N. A. Elkouh, S. Murray, and D. L. Chubb, “Thermophotovoltaic converter performance for radioisotope power systems,” in *AIP Conference Proceedings: Space Technology and Applications International Forum* (AIP, 2005), pp. 601–614.
 45. W. Chan, R. Huang, C. A. Wang, J. Kassakian, J. D. Joannopoulos, and I. Celanovic, “Modeling low-bandgap thermophotovoltaic diodes for high-efficiency portable power generators,” *Sol. Ener. Mater. Sol. Cells* **94**, 509–514 (2010).
 46. E. R. G. Eckert and E. M. Sparrow, “Radiative heat exchange between surfaces with specular reflection,” *Int. J. Heat Mass Trans.* **3**, 42–54 (1961).
 47. J. Nelson, *The Physics of Solar Cells* (Imperial College Press, 2003).
 48. A. Taflov and S. C. Hagness, *Computational Electrodynamics: The Finite-Difference Time-Domain Method* (Artech House, 2000).
 49. J. Bravo-Abad, F. J. García-Vidal, and L. Martín-Moreno, “Resonant transmission of light through finite chains of subwavelength holes in a metallic film,” *Phys. Rev. Lett.* **93**, 227401 (2004).
 50. Y. S. Touloukian and D. P. DeWitt, “Thermal Radiative Properties: Metallic Elements and Alloys,” in *Thermophysical Properties of Matter Volume 7* (IFI/PLENUM, 1970).
 51. NREL, “Best Research-Cell Efficiencies Chart,” http://www.nrel.gov/ncpv/images/efficiency_chart.jpg.
 52. C. H. Henry, “Limiting efficiencies of ideal single and multiple energy gap terrestrial solar cells,” *J. Appl. Phys.* **51**, 4494–4500 (1980).
 53. W. Shockley and H. J. Queisser, “Detailed balance limit of efficiency of p-n junction solar cells,” *J. Appl. Phys.* **32**, 510–519 (1961).
 54. L. M. Fraas and L. Minkin, “TPV history from 1990 to present & future trends,” *AIP Conf. Proc.* **890**, 17–23 (2007).

1. Introduction

Recent advancements in the field of low bandgap photovoltaic (PV) cells [1–4] has led to renewed interest in developing high efficiency and high power density thermophotovoltaic (TPV) energy conversion systems, whereby direct conversion of thermal radiation to electricity is

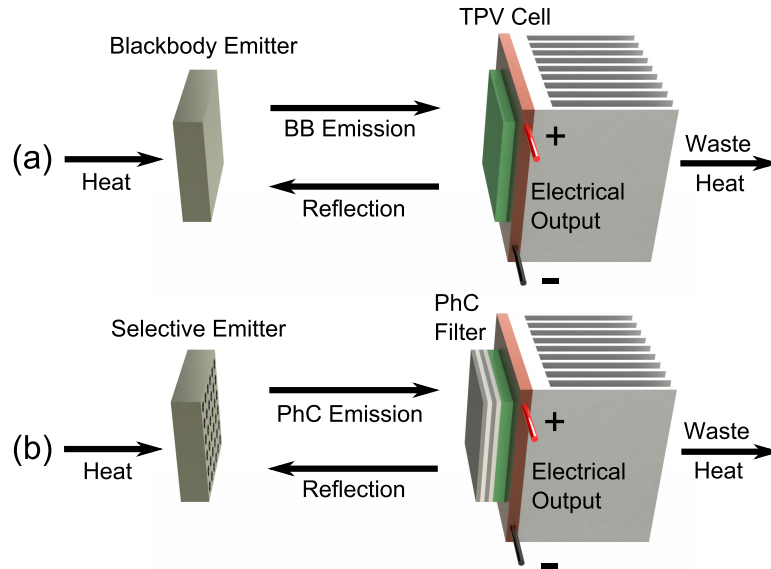


Fig. 1. (a) Conventional thermophotovoltaic (TPV) energy conversion system without spectral control. (b) TPV system with 2D photonic crystal (PhC) selective emitter and cold side filter. Spectral control enables performance enhancement of up to 400% over the conventional TPV system.

achieved via the PV effect [5–7]. Compared to solar PV conversion, the heat source is significantly closer to the PV cell, resulting in photon flux and power density that is orders of magnitude higher. However, due to the much lower temperatures achievable in practical TPV systems (< 2000 K), the majority of emitted photons lie in the near- to mid-infrared spectrum, hence the importance of high quality low bandgap PV cells in developing high efficiency TPV systems. TPV systems offer many advantages, including the promise of highly versatile and compact high power density energy conversion systems that have no moving parts, leading to quiet and robust operation. Virtually any high grade heat source can be utilized, including waste heat [7], fossil fuels [8], radioisotopes [9, 10], and solar energy [11, 12].

Even though low bandgap PV cells allow more efficient use of the emitted radiation, the broadband nature of thermal emission at the relatively low temperatures considered results in significant emission of below bandgap photons. For instance, only 28% of the radiant exitance of a blackbody at 1500 K with peak radiation at a wavelength of $1.93 \mu\text{m}$ lies below $2 \mu\text{m}$, which is approximately the bandgap of InGaAs PV cells [3, 13]. The remaining non-convertible photons emitted result in parasitic heat losses, which would also lead to highly undesirable elevated PV cell operating temperatures. Hence, spectral control is critical in achieving higher TPV system efficiencies.

Spectral control can be achieved firstly via the use of selective emitters to preferentially emit convertible photons. To date, various selective emitters have been investigated; from rare-earth oxides [14–17], to 1D [18, 19], 2D [20–25], and 3D photonic crystals (PhCs) [26, 27]. Another spectral control approach relies on recuperating non-convertible photons using front surface reflectors [28–31] and back surface reflectors [32–34] on the PV cell. A TPV system including both aspects of spectral control is shown in Fig. 1(b).

Following recent efforts on the design, fabrication, characterization, and optimization of spectral control devices for TPV applications, many studies have attempted to estimate the

enhancement in TPV system performance [8, 35–37]. In this investigation, we focus on obtaining estimates of TPV system performance using spectral control components that have recently been demonstrated *experimentally* while taking into account high temperature and angular dispersion properties to ensure realistic estimates. In particular, we focus on 2D tantalum (Ta) PhCs as the selective emitter; this design enables a sharp emittance cutoff that is easily shifted and optimized [24, 38, 39], is scalable to large areas [40, 41], and has been proven to be thermally stable at high temperatures in high vacuum conditions [42]. The performance of this emitter is evaluated with or without a cold side tandem filter [28, 31], which to date is widely regarded as one of the more promising experimentally realized reflective spectral control device [29, 43, 44].

In the following section, we discuss the numerical model used to obtain detailed performance predictions of TPV systems. Inputs to the model include key physical properties of each component that constitute the TPV system; optical properties are captured by the absorptance, reflectance, and transmittance of the emitter, cold side filter, and PV cell; electrical power generating properties are captured by the quantum efficiency, dark current, parasitic resistances, and ideality factor of the PV cell. Methods to obtain optimized 2D Ta PhC selective emitter and cold side tandem filter designs are also discussed. In section 3, TPV modeling results of various emitter and cold side filter combinations are presented. In addition, we analyze the performance of 3 different current state-of-the-art low bandgap TPV cells using key physical properties that have been experimentally measured from fabricated cells; GaSb [2, 45], InGaAs [3, 13], and InGaAsSb [1, 4, 45]. The results using experimentally realizable components are benchmarked against idealized components to identify areas that require improvement. We conclude by summarizing our findings in section 4.

2. Numerical model

2.1. Thermophotovoltaic (TPV) system

To obtain the short circuit current I_{sc} generated, the net irradiance incident on the PV cell is calculated following a ray tracing approach. We begin with the definition of the spectral radiance of a blackbody i_{BB} :

$$i_{BB}(\lambda, T) = \frac{2hc^2}{\lambda^5 [\exp(\frac{hc}{\lambda kT}) - 1]} \quad (1)$$

where λ is the wavelength, h is Planck's constant, c is the speed of light, k is Boltzmann's constant, and T is the temperature of the blackbody. The total radiant power emitted P_{em} by an emitter of area A_1 with angular dependent emittance $\varepsilon(\lambda, \theta_1, \phi_1)$ at temperature T is then given by:

$$P_{em} = \int_0^\infty d\lambda \int_0^{\frac{\pi}{2}} d\theta_1 \int_0^{2\pi} d\phi_1 \int_{A_1} dA_1 [i_{BB}(\lambda, T) \varepsilon(\lambda, \theta_1, \phi_1) \cos \theta_1 \sin \theta_1] \quad (2)$$

where θ_1 is the polar angle and ϕ_1 is the azimuthal angle.

The fraction of P_{em} reaching the PV cell can be evaluated by first considering the differential radiant power incident on the PV cell of infinitesimal area dA_2 from an emitter of infinitesimal area dA_1 :

$$dQ_{dA_1 \rightarrow dA_2} = i_{BB}(\lambda, T) \varepsilon(\lambda, \theta_1, \phi_1) dA_1 dF_2 \quad (3)$$

dF_2 is the differential view factor, which is defined as the fraction of radiant energy emitted by dA_1 incident on dA_2 :

$$dF_2 = \frac{\cos \theta_1 \cos \theta_2}{s^2} dA_2 \quad (4)$$

where θ_2 is the angle between the straight line connecting the two infinitesimal areas and the normal vector for dA_2 , and s is the distance between dA_1 and dA_2 .

In a TPV system, it is important to take into account the multiple reflections taking place between the emitter and the PV cell. It is thus convenient to define the differential view factor dF_l for dA_l , a differential virtual surface area constructed at a distance s_l from the initial emitter dA_1 to properly take into account the l th order reflection [46]:

$$dF_l = \frac{\cos \theta_1 \cos \theta_l}{s_l^2} dA_l \quad (5)$$

Even values of l represent reflections to the PV cell, while odd values represent reflections back to the emitter. Thus, the radiant power reabsorbed P_{re} by the emitter can be evaluated by integrating Eq. (3) and summing over the odd values of l :

$$P_{re} = \sum_{p=1}^{\infty} \int d\lambda \int dF_{2p+1} \int dA_1 \left[i_{BB}(\lambda) R_2^p R_1^{p-1} (1 - R_1) \varepsilon(\lambda, \theta_{2p+1}, \phi_{2p+1}) \right] \quad (6)$$

where R_1 and R_2 are the angular dependent reflectance of the emitter and the PV cell respectively. The terms $R_2^p R_1^{p-1}$ and $1 - R_1$ respectively captures the multiple reflections and final absorption events. For a parallel plate TPV system configuration considered in this investigation, Eq. (6) can be further simplified to the following:

$$P_{re} = \sum_{p=1}^{\infty} \int d\lambda \int dA_{2p+1} \int dA_1 \left[\frac{i_{BB}(\lambda) R_2^p R_1^{p-1} (1 - R_1) \varepsilon(\lambda, \theta_{2p+1}, \phi_{2p+1}) \cos^2 \theta_{2p+1}}{s_{2p+1}^2} \right] \quad (7)$$

Similarly, the useful radiant power incident on the PV cell P_{cell} , and I_{sc} can be obtained by summing over the even values of l :

$$P_{cell} = \sum_{p=1}^{\infty} \int_0^{\lambda_g} d\lambda \int dA_{2p} \int dA_1 \left[\frac{i_{BB} (R_1 R_2)^{p-1} (1 - R_2) \varepsilon(\lambda, \theta_{2p}, \phi_{2p}) \cos^2 \theta_{2p}}{s_{2p}^2} \right] \quad (8)$$

$$I_{sc} = 2qc \sum_{p=1}^{\infty} \int \frac{IQE(\lambda) d\lambda}{\lambda^4 [\exp(\frac{hc}{\lambda kT}) - 1]} \int dA_{2p} \int dA_1 \left[\frac{(R_1 R_2)^{p-1} (1 - R_2) \varepsilon(\lambda, \theta_{2p}, \phi_{2p}) \cos^2 \theta_{2p}}{s_{2p}^2} \right] \quad (9)$$

where $IQE(\lambda)$ and λ_g are respectively the internal quantum efficiency and bandgap of the PV cell. Equation (9) is then used to evaluate the total output current I as a function of applied voltage V at the output terminals of the PV cell according to:

$$I = I_{sc} - I_o \exp \left[\frac{q(V + IR_s)}{mkT_c} \right] - \frac{V + IR_s}{R_{sh}} \quad (10)$$

where m , I_o , R_s , R_{sh} , and T_c are respectively the ideality factor, dark current, series resistance, shunt resistance, and temperature of the PV cell, and q is the elementary electronic charge [47]. The output electrical maximum power point $P_{elec, max}$ is then obtained by maximizing $P_{elec} = IV$ by setting $d(IV)/dV = 0$. The radiant heat-to-electricity TPV efficiency η_{TPV} is then given as follows:

$$\eta_{TPV} = \frac{P_{elec, max}}{P_{em} - P_{re}} \quad (11)$$

η_{TPV} can further be broken down into the overall spectral efficiency when TPV cavity effects are taken into account $\eta_{Cav-Spec}$, and the PV cell efficiency η_{Cell} :

$$\eta_{Cav-Spec} = \frac{P_{cell}}{P_{em} - P_{re}} \quad (12)$$

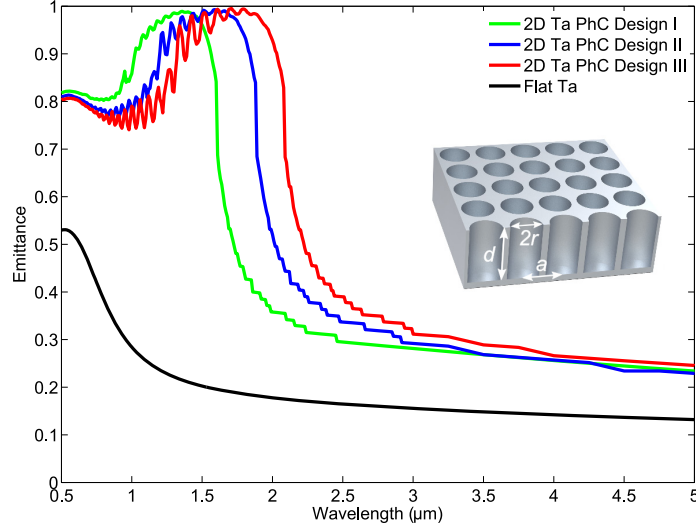


Fig. 2. Simulated high temperature ($T = 1478$ K) normal spectral emittance of flat Ta and 2D Ta PhCs optimized for GaSb (Design I: $r = 0.43$ μm , $d = 8.00$ μm , $a = 0.95$ μm), InGaAs (Design II: $r = 0.51$ μm , $d = 8.00$ μm , $a = 1.11$ μm), and InGaAsSb (Design III: $r = 0.57$ μm , $d = 8.00$ μm , $a = 1.23$ μm). As can be seen, the cutoff is easily shifted by modifying the dimensions of the PhC.

$$\eta_{\text{Cell}} = \frac{P_{\text{elec, max}}}{P_{\text{cell}}} \quad (13)$$

Note that the evaluation of Eqs. (7)–(9) can be computationally intensive, especially in obtaining estimates for optimization purposes. Thus, it is interesting to consider the simplification of capturing the angular dependence via the spectral hemispherical emittance $\varepsilon_{\text{H}}(\lambda)$:

$$\varepsilon_{\text{H}}(\lambda) = \frac{1}{\pi} \int_0^{\frac{\pi}{2}} d\theta_1 \int_0^{2\pi} d\phi_1 [\varepsilon(\lambda, \theta_1, \phi_1) \cos \theta_1 \sin \theta_1] \quad (14)$$

Using this, the problem simplifies into radiation exchange between two general surfaces of total area A_1 and A_2 , thereby not requiring the intensive numerical integration over all differential areas. Indeed, we have verified that both the full ray tracing method and the spectral hemispherical approximation produce results that agree very well. This is expected given the very high view factors (> 0.85) involved in practical parallel plate TPV systems that are considered in this investigation, whereby most emission up to $\theta_1 = 85^\circ$ is incident on the PV cell.

2.2. Two-dimensional (2D) tantalum (Ta) photonic crystals (PhCs) as selective emitters

To achieve a highly efficient TPV system, the emitter should exhibit maximum emission at wavelengths below the cutoff of the PV cell, whilst simultaneously suppressing emission in the non-convertible range. In addition, the emitter has to survive high temperature operation of up to 1500 K over extended periods of time, thus limiting the materials and architectures that can be used in these systems.

To overcome these critical issues, we select a material platform consisting of single element, broadband tunable spectrally selective infrared emitters comprised of a 2D square array of cylindrical cavities with period a , radius r , and depth d etched into a large area metallic surface as shown in the inset of Fig. 2. This relatively simple design allows one to simultaneously achieve near-blackbody emittance at short wavelengths as well as emittance almost as low as

a polished metal at long wavelengths, with a sharp cutoff separating the two regimes, which is critical for high efficiency TPV energy conversion. Of the various refractory metals available, tantalum (Ta) is an excellent choice given its low vapor pressure, high melting point, machinability and weldability. To date, the 2D Ta PhC emitter has been demonstrated to be thermally stable at high temperatures in high vacuum environments [42], and the fabrication process is scalable to large areas [40, 41], both of which are essential for practical large scale adoption.

In general, the enhancement in emission is achieved by coupling into resonant cavity electromagnetic modes, whereby the cutoff wavelength is approximately given by the fundamental mode of the cylindrical metallic cavity [22–24]. Hence, the cutoff wavelength is mainly affected by r , with d playing only a secondary role for the aspect ratios considered. To further enhance the selective emitter's performance, the appropriate r , d and a are selected such that the radiative and absorptive rates of the metallic cavities are matched, i.e. satisfying the Q-matching condition [38]. This allows the PhC to exhibit emittance peaks that approach the theoretical blackbody in the vicinity of the fundamental mode.

While Q-matching of the fundamental mode allows quick identification of near-optimal designs for TPV systems, it is not the global optimum as it is difficult to simultaneously achieve Q-matching for higher order modes, which is important in broadening the bandwidth for maximum emittance. Hence, global optimization using numerical methods is employed [37], with the design provided by Q-matching of the fundamental mode used as the initial estimate.

The emittance $\varepsilon(\lambda, \theta_1, \phi_1)$ of the 2D Ta PhC can easily be determined via finite-difference time-domain (FDTD) numerical methods [48] coupled with the Lorentz–Drude model fitted to elevated temperature emittance [42] to capture the optical dispersion of Ta. However, the high memory requirements and slow computational speed of FDTD methods limit its application in determining the globally optimum design for a TPV system. Thus, to obtain quicker estimates, we utilize the mode matching formalism described in [49] by Bravo-Abad *et al.*, of which we have confirmed to match very well with FDTD methods. In essence, the reflectance is calculated by matching the radiation fields at the boundary of free space and the cylindrical cavities via expansion of the cavity modes for shorter wavelengths and utilizing a surface area weighted impedance for longer wavelengths.

The calculated $\varepsilon(\lambda, \theta_1, \phi_1)$ can then be used to obtain η_{TPV} and the maximum power density $J_{\text{elec,max}} = P_{\text{elec,max}}/A_1$ as described in Section 2.1. For optimization purposes, we define the figure of merit FOM as follows:

$$\text{FOM} = x\eta_{\text{TPV}} + (1-x)\frac{J_{\text{elec,max}}^{\text{PhC}}}{J_{\text{elec,max}}^{\text{BB}}} \quad (15)$$

where $J_{\text{elec,max}}^{\text{PhC}}/J_{\text{elec,max}}^{\text{BB}}$ captures the TPV system power density performance of the 2D Ta PhC emitter compared to a blackbody, and x is the weighting given to η_{TPV} in the optimization routine, which could be modified depending on design goals. In this investigation, we are mainly concerned in obtaining the highest η_{TPV} possible, thus $x = 0.9$ is used. Using this, 3 different designs optimized for GaSb [2, 45], InGaAs [3, 13], and InGaAsSb [1, 4, 45] cells are obtained. As can be seen in Fig. 2, the normal incidence spectral emittance of the optimized 2D Ta PhCs is high at wavelengths below the bandgap of the respective TPV cells, and low in the non-convertible wavelength range. Note that in the optimization routine, we assume an approximate operating T of 1500 K and a fixed view factor $F = 0.99$, which is realistically achievable using a 10 cm \times 10 cm flat plate geometry with separation $s = 500 \mu\text{m}$. Regardless, the exact operating T and F of the final optimal TPV system is relatively unimportant as long as they are reasonably close. This is due to the fact that the optimization routine indirectly searches for the design with the best selective normal and hemispherical emittance. Note that we have also limited d to 8.00 μm for ease of fabrication [41].

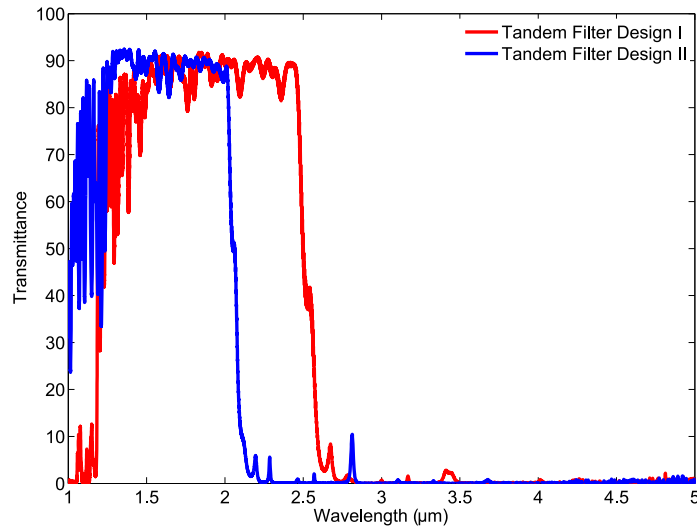


Fig. 3. Measured normal incidence transmittance of tandem filters optimized for 0.5 eV and 0.6 eV TPV cells. The tandem filters consist of dielectric stacks of antimony selenide (Sb_2Se_3) and yttrium fluoride (YF_3), terminated with a $1\ \mu\text{m}$ thick heavily doped indium phosphide arsenide (InPAs) layer as the plasma filter. The tandem filters are sourced from Rugate Technologies, Inc.

2.3. Plasma-dielectric stacks as cold side bandpass filters

Recent TPV system experiments demonstrating record η_{TPV} of 19% employed a greybody-like graphite emitter with a cold side tandem filter [44]. It is thus instructive to compare the TPV system performance using 2D Ta PhCs as the emitter, with or without the tandem filter.

The tandem filter consists of bi-material multilayer dielectric stack terminated with a plasma filter [28,31]. The dielectric stack exhibits high transmission for photons within the convertible range yet simultaneously providing high reflection in the mid-infrared range ($\lambda \sim 2\text{--}6\ \mu\text{m}$). A plasma filter consisting of a highly doped semiconductor placed at the end of the multilayer dielectric stack extends the bandwidth of high reflection beyond $\lambda = 6\ \mu\text{m}$. The cutoff can be shifted by modifying the thicknesses of the dielectric stack layers, and further optimized for particular TPV cells using the optimization technique described in [28] by Rahmlow *et al.* The measured normal incidence transmittance of two particular designs optimized for 0.5 eV and 0.6 eV cutoffs are shown in Fig. 3. The filters are fabricated by Rugate Technologies, Inc. using antimony selenide (Sb_2Se_3) and yttrium fluoride (YF_3) as the multilayer dielectric stack, and a heavily doped indium phosphide arsenide (InPAs) layer as the plasma filter.

3. Results and discussion

We now consider TPV systems utilizing both the optimized 2D Ta PhC selective emitter and the cold side tandem filter discussed in Section 2.2 and Section 2.3 respectively. To benchmark the performance of the 2D Ta PhC selective emitter, a greybody emitter ($\epsilon = 0.9$) and an idealized cutoff emitter ($\epsilon_{\text{H}} = 0.9$ for wavelengths smaller than the cutoff and $\epsilon_{\text{H}} = 0.1$ for wavelengths larger than the cutoff) are included in the analysis. The idealized cutoff emitter is used as the approximate upper limit achievable with metallic PhCs. The effect of temperature T , view factor F , and below bandgap emission of selective emitters on system efficiency are also explored. Since these trends are general for all TPV cells in consideration, we only present results for the

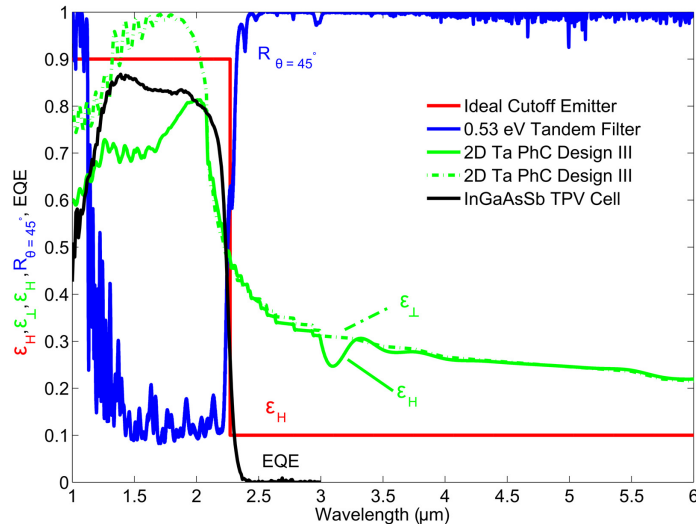


Fig. 4. Relevant optical properties for optimized components in an InGaAsSb TPV system. The normal incidence emittance ϵ_{\perp} and hemispherical emittance ϵ_H of the optimized 2D Ta PhC emitter, and 45° reflectance $R_{\theta=45^\circ}$ of the 0.53 eV tandem filter is shown to match the external quantum efficiency (EQE) of InGaAsSb. An ideal cutoff emitter is included in the analysis to elucidate the effect of non-ideal spectral emittance of the optimized 2D Ta PhC.

particular InGaAsSb TPV cell described in [45] by Chan *et al.* Finally, we elucidate the effects of TPV cell non-idealities, and present estimates of optimized TPV system efficiencies using GaSb [2,45], InGaAs [3,13], and InGaAsSb [1,4,45] TPV cells, as well as compare the results to notable TPV experimental results reported to date.

3.1. Optimized InGaAsSb TPV system

Figure 4 presents the measured external quantum efficiency (EQE) of the fabricated InGaAsSb cells [45], together with the normal (ϵ_{\perp}) and hemispherical emittance (ϵ_H) of the optimized 2D Ta PhC. As can be seen, the cutoff of the emittance matches well with the EQE of the InGaAsSb TPV cell. Although the performance is excellent at normal incidence, ϵ_H is significantly lower in the region of high EQE, which would negatively impact both η_{TPV} and $J_{\text{elec,max}}$ since typical TPV systems are operated at high view factors.

The intrinsic angular selectivity of the 2D Ta PhC arises from the constancy of the resonant peaks and the decreasing diffraction threshold as a function of incident polar angle. At wavelengths below the diffraction threshold, absorptance decreases because there are more channels to reflect back to and the radiative Q decreases, thus destroying Q-matching. Therefore, at larger incident polar angles, the in-band absorption region decreases and has a lower average absorptance (see Fig. 4). Nevertheless, ϵ_H still approaches the long wavelength limit determined by the volume fraction of air to Ta, thus maintaining some degree of spectral selectivity.

The tandem filter also suffers from angular dispersion detrimental to TPV systems. However, variations in the magnitude of transmittance for wavelengths smaller than the cutoff and reflectance for wavelengths larger than the cutoff are less severe compared to the optimized 2D Ta PhCs. As θ increases, the cutoff shifts to smaller wavelengths; selectivity only starts degrading above $\theta = 60^\circ$ [28]. Hence, the spectral hemispherical reflectance of the tandem filter is closely approximated by $\theta = 45^\circ$ reflectance, $R_{\theta=45^\circ}$. Since spectral hemispherical reflectance

measurements of optimized filters are not available, shifted versions of measured normal incidence transmittance of filters shown in Fig. 3 are used as an estimate for $R_{\theta=45^\circ}$ in order to obtain estimates of η_{TPV} for systems employing the tandem filter. This is reasonable given that the cutoff of the filter is easily shifted within the wavelength range of interest in TPV by altering the layers' thicknesses, $R_{\theta=45^\circ}$ closely approximates normal incidence reflectance, and the filter exhibits absorptance close to zero for $\lambda = 1\text{--}9\ \mu\text{m}$ [28]. The estimated $R_{\theta=45^\circ}$ for a 0.53 eV tandem filter optimized for InGaAsSb TPV cells is shown in Fig. 4.

For TPV systems without the optimized tandem filter, the reflectance of the bare InGaAsSb cell becomes critical. Hence, reflectance of the InGaAsSb cells are included whenever possible, i.e. extracted from data published in literature [45]. Nevertheless, due to the limited wavelength range where reflectance data is available, we assume zero reflectance at wavelengths where data is unavailable to ensure conservative η_{TPV} estimates. We also assume a constant reflectance for the TPV cells over all angles as published literature data for experimentally fabricated cells are limited to near normal incidence. Regardless, these approximations do not prevent us from exposing critical spectral control requirements necessary in engineering efficient TPV systems, which is the main objective of this investigation.

3.2. Effect of temperature and view factor

Using the numerical model presented in Section 2, η_{TPV} can be estimated for InGaAsSb TPV systems comprising the ideal cutoff selective emitter, 2D Ta PhC selective emitter, or greybody emitter ($\varepsilon = 0.9$), with or without the optimized tandem filter. First, we consider a system with a fixed $F = 0.99$. As shown in Fig. 5(a), there exists an optimum operating T for each of the combinations considered; if T is too low, the emission peak is located at wavelengths smaller than the bandgap of the TPV cell as indicated by sub-optimal $\eta_{\text{Cav-Spec}}$ and η_{Cell} shown in Figs. 5(b) & (c); if T is too high, the TPV cell's series resistance losses dominate as indicated by the reduction in η_{Cell} shown in Fig. 5(c).

At the optimum T , highest η_{TPV} is achieved by including the optimized 0.53 eV tandem filter; coupling the filter with the greybody and 2D Ta PhC emitter results in a maximum efficiency $\eta_{\text{TPV,max}}$ of 23.5% and 23.7% respectively, which is extremely close to the performance of the ideal cutoff emitter of $\eta_{\text{TPV,max}} = 24.3\%$. The optimum operating temperatures are 1260 K, 1230 K, and 1210 K for the 2D TaPhC, greybody, and ideal cutoff emitter respectively, when coupled with the tandem filter. For all three cases, power density is approximately $0.62\ \text{W cm}^{-2}$. The results however indicate that in a high F system, the use of a selective emitter is not critical if an optimized tandem filter is present. This is mainly due to the tandem filter's steep cutoff and high reflectance below the bandgap. Nevertheless, if implementation of the filter is not possible, the optimized 2D Ta PhC emitter offers $> 70\%$ improvement in $\eta_{\text{TPV,max}}$ over the greybody emitter.

To further study the effect of F , we consider each of the combinations at their optimum T . As shown in Fig. 6 the greybody performs as well as the optimized 2D Ta PhC when coupled with the optimized tandem filter at $F > 0.97$ ($10\ \text{cm} \times 10\ \text{cm}$ flat plate geometry with separation $s < 1.7\ \text{mm}$). If $F < 0.97$, significant improvement is seen with the optimized 2D Ta PhC over the greybody as the efficiency of photon recycling using the tandem filter deteriorates. Note also that in practical systems, F is limited by the reduction in active cell area due to front side metallization requirements of the TPV cells.

3.3. Effect of non-ideal selective emitter

As can be seen in Fig. 5, a selective emitter is critical for TPV systems without the optimized tandem filter. It is also observed that the optimized 2D Ta PhC emitter does not come close to achieving the performance of the ideal cutoff emitter. This is primarily due to long wavelength

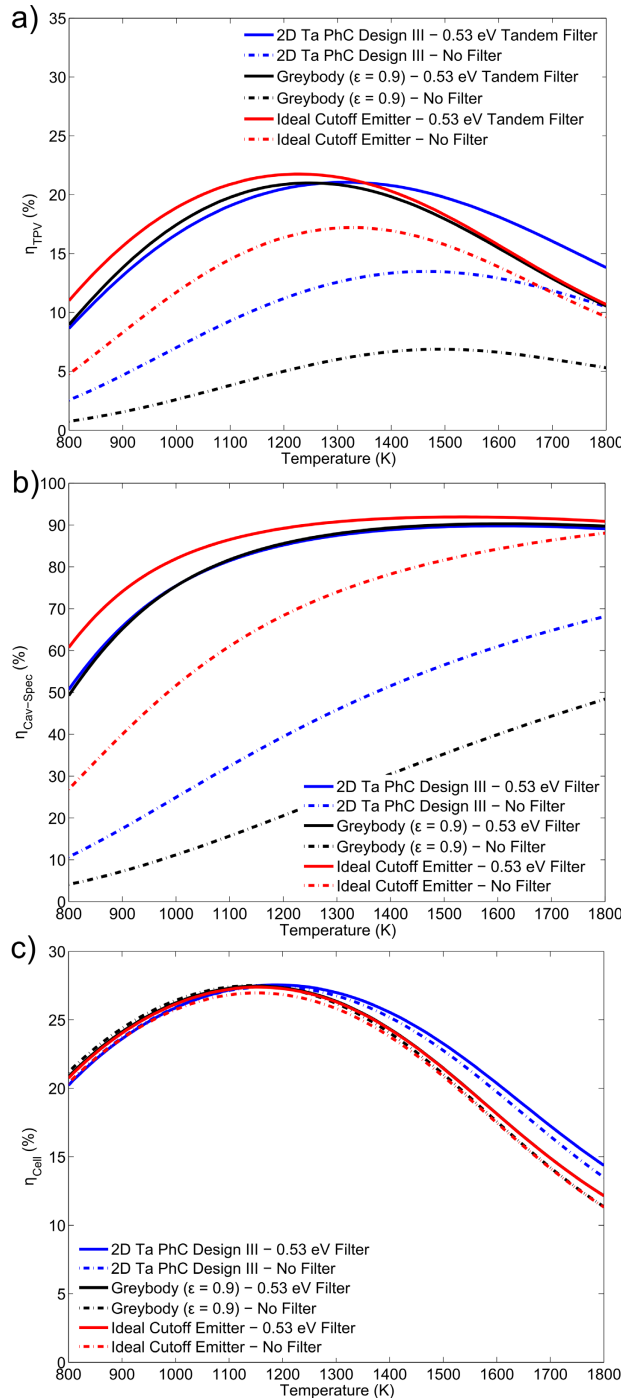


Fig. 5. (a) Radiant heat-to-electricity η_{TPV} for various emitters with or without an optimized tandem filter in combination with InGaAsSb TPV cell at fixed view factor $F = 0.99$ ($10 \text{ cm} \times 10 \text{ cm}$ flat plate geometry with separation $s = 500 \mu\text{m}$). An optimum temperature T exist for each combination. Due to considerable emission below the bandgap of the InGaAsSb TPV cell for the emitters considered, significant improvement is seen with the use of the tandem filter. (b) Overall spectral efficiency when TPV cavity effects are included, $\eta_{Cav-Spec}$. When $F = 0.99$, use of a selective emitter is not critical if an optimized tandem filter is present. (c) TPV cell efficiency η_{Cell} . For $T > 1200 \text{ K}$, degradation of η_{Cell} is seen

#195203, \$15.00 USD, Received 6 Aug 2013; revised 10 Sep 2013; accepted 1 Oct 2013; published 17 Oct 2013
 due to Optics Express series being made available via CrossRef. Check latest version of CrossRef.org for article corrections.

(C) 2013 OSA 4 November 2013 | Vol. 21, No. S6 | DOI:10.1364/OE.21.0A1035 | OPTICS EXPRESS A1046

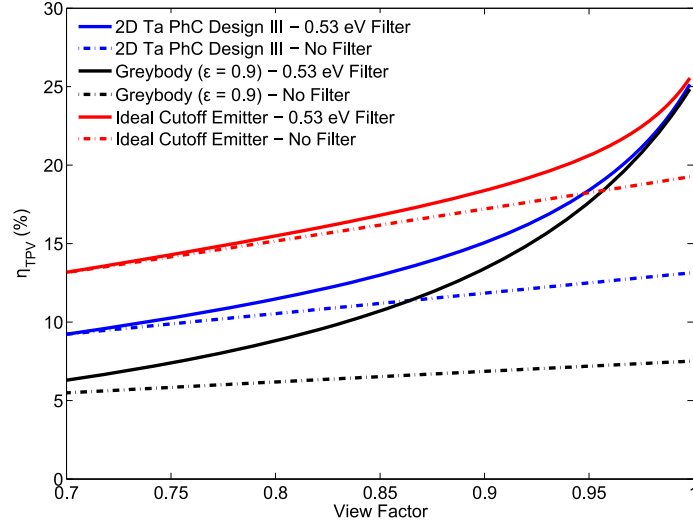


Fig. 6. With T fixed at the optimum, the most efficient combination depends on the experimentally achievable F . For $F > 0.97$ (10 cm \times 10 cm flat plate geometry with separation $s < 1.7$ mm), the use of the optimized tandem filter allows the greybody to slightly outperform the optimized 2D Ta PhC selective emitter. In contrast, it is important to restrict below bandgap emission via selective emitters in TPV systems with smaller view factors.

emittance that is larger by a factor of two compared to the ideal cutoff emitter, which is inevitable even with a low emissivity polished metal given that intrinsic free electron damping losses significantly increase with the rise of temperature [50]. The question now lies as to how much improvement can be seen if the long wavelength emission can be suppressed to hypothetical levels in future selective emitter development. To study this, we compare the performance of a greybody emitter to an ideal cutoff selective emitter, with above bandgap hemispherical emittance $\epsilon_{sw} = 0.9$, and a varying below bandgap hemispherical emittance ϵ_{lw} . Estimates of η_{TPV} for both emitters at $T = 1250$ K (which is approximately the optimum for InGaAsSb TPV) with or without the 0.53 eV optimized tandem filter are presented in Figs. 7(a) and 7(b) for $F = 0.99$ and $F = 0.97$ respectively.

As can be seen, use of a selective emitter results in markedly increased η_{TPV} over a greybody if the optimized tandem filter is absent. Notice that a larger relative improvement in η_{TPV} is seen compared to the relative reduction in ϵ_{lw} . However, for a TPV system using only the ideal cutoff emitter for spectral control, ϵ_{lw} must be smaller than 0.03 to outperform the greybody – optimized tandem filter combination. Thus, effective spectral control is more readily attainable using the cold side optimized tandem filter compared to the hot side selective emitter in high F TPV systems. If $F < 0.97$, both aspects of spectral control become important; a relative improvement $> 10\%$ over the greybody emitter is realized for $\epsilon_{lw} < 0.1$ when used in combination with the optimized tandem filter.

3.4. Effect of non-ideal TPV cells

From 1975 to 2000, efficiencies of silicon PV cells under AM1.5G solar irradiance have more than doubled from 13% to 25% [51]. In fact, the latest state of the art silicon PV cells approach $\sim 85\%$ of their theoretical thermodynamic limit [52], a feat made even more impressive given that silicon has an indirect bandgap. It is thus reasonable to envision a similar path followed by direct low bandgap TPV cells if similar research efforts are undertaken, upon which would lead

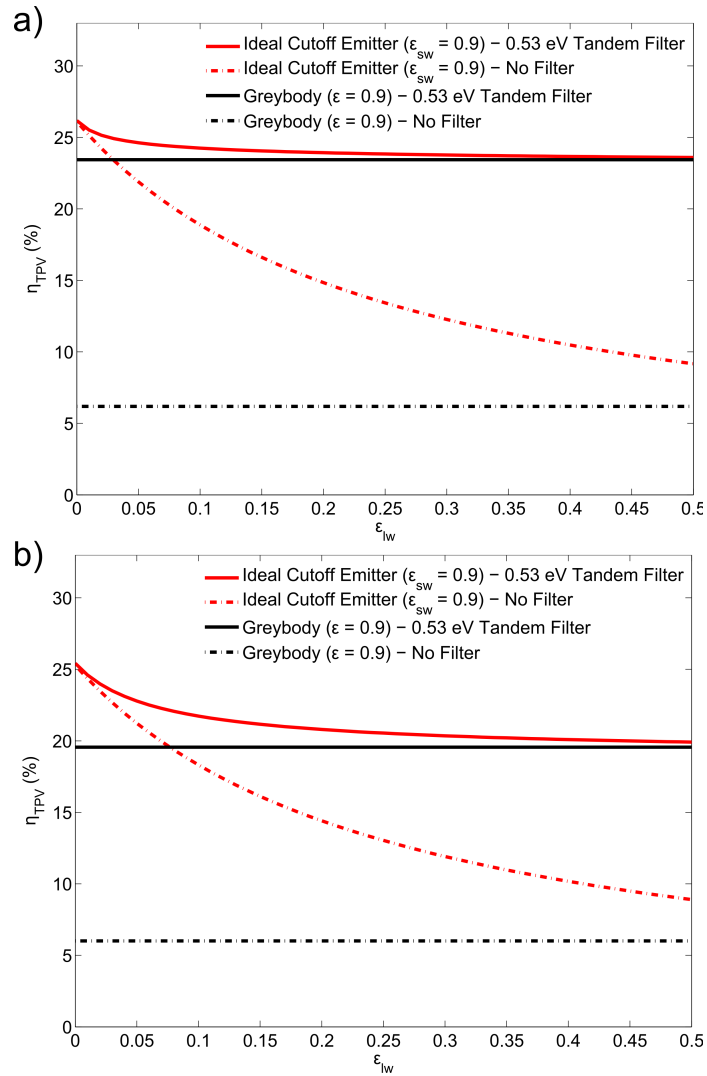


Fig. 7. η_{TPV} for an InGaAsSb TPV system including an ideal cutoff emitter with varying below bandgap hemispherical emittance ϵ_{lw} with or without a 0.53 eV optimized tandem filter at a fixed temperature T of 1250 K. (a) $F = 0.99$. To outperform the greybody - optimized tandem filter combination, ϵ_{lw} must be smaller than 0.03, to a point where addition of the tandem filter is detrimental given the larger reduction in power density for a small improvement in η_{TPV} . (b) $F = 0.97$. To outperform the greybody - optimized tandem filter combination, ϵ_{lw} must be smaller than 0.08. As F is reduced, both aspects of spectral control become important.

Table 1. Predicted $\eta_{\text{TPV,max}}$ for three different TPV cells utilizing experimentally realizable spectral control components at fixed $F = 0.99$. Optimum temperature indicated in brackets is determined for each TPV system combination using fabricated and characterized TPV cells (GaSb [45], InGaAs [3], and InGaAsSb [45]). Results indicate that current state of the art fabricated TPV cells are $\sim 50\%$ as efficient as their thermodynamically ideal counterparts. It is also interesting to note that spectral control via the optimized 2D Ta PhC and tandem filter enables TPV cells with larger bandgaps (GaSb) to perform as well as TPV cells with smaller bandgaps (InGaAsSb). However, the use of smaller bandgap TPV cells would result in lower optimum temperatures.

TPV System	Predicted $\eta_{\text{TPV,max}}(\%)$					
	GaSb		InGaAs		InGaAsSb	
	Fabricated Cell [45]	Ideal Cell	Fabricated Cell [3]	Ideal Cell	Fabricated Cell [45]	Ideal Cell
Optimized 2D Ta PhC & Tandem Filter	22.8% (1390 K)	45.9% (1390 K)	25.0% (1320 K)	45.7% (1320 K)	23.7% (1260 K)	45.0% (1260 K)
Greybody ($\epsilon = 0.9$) & Tandem Filter	22.3% (1360 K)	45.6% (1360 K)	24.8% (1290 K)	45.5% (1290 K)	23.5% (1230 K)	45.4% (1230 K)
Optimized 2D Ta PhC	9.2% (1560 K)	23.3% (1560 K)	12.8% (1470 K)	26.0% (1470 K)	13.0% (1440 K)	29.1% (1440 K)
Greybody ($\epsilon = 0.9$)	4.5% (1570 K)	12.6% (1570 K)	7.0% (1490 K)	15.1% (1490 K)	7.5% (1470 K)	18.7% (1470 K)

to significantly higher η_{TPV} .

To quantify the possible increase in η_{TPV} , we consider TPV cells limited only by thermalization losses and radiative recombination, i.e. the Shockley-Queisser limit [53]. This is easily implemented in the model described in Section 2.1 by setting $R_s = 0$, $R_{\text{sh}} = \infty$, and $m = 1$ in Eq. 10. In addition, I_0 is set to the thermodynamic limit determined solely by radiative recombination [52]:

$$I_0 = \frac{A_2 q (n^2 + 1) E_g^2 k T_c}{4\pi^2 \hbar^3 c^2} \exp(-E_g/kT_c) \quad (16)$$

where n is the refractive index of the TPV semiconductor region, E_g is the energy gap of the TPV cell, and $\hbar = h/2\pi$. Lastly, the ideal TPV cell is assumed to possess an $\text{EQE}(\lambda)$ of 1 for wavelengths smaller than the bandgap and 0 for wavelengths larger than the bandgap. Using this, predicted η_{TPV} for all emitter-filter-TPV cell combinations are obtained and are presented in Table 1. Note that the 2D Ta PhC selective emitters, tandem filter, and T indicated in brackets are optimized for current state of the art low bandgap TPV cells (GaSb [45], InGaAs [3], and InGaAsSb [45]). In this analysis, we have also neglected the contribution of reabsorption of photons generated by radiative recombination in the TPV cells by the emitter, since it is much smaller than P_{em} , and that typical maximum power operation extracts $> 90\%$ of the photocurrent generated. If this contribution is included, we expect $< 5\%$ relative increase in η_{TPV} estimates for the ideal cell.

As can be seen in Table 1, current state of the art fabricated TPV cells are $\sim 50\%$ as efficient as their thermodynamically ideal counterparts. For the InGaAsSb TPV system utilizing the optimized tandem filter and the optimized 2D Ta PhC selective emitter at the optimum operating $T = 1260$ K, $\sim 12\%$, $\sim 28\%$, and $\sim 13\%$ of the losses are attributable to non-ideal EQE, non-radiative recombination mechanisms, and series resistance respectively. Series resistance is also the main cause of lower optimum operating T . As T approaches 1800 K, the proportion of losses attributable to series resistance increases to $\sim 40\%$.

The most efficient TPV system that can be assembled today consists of the experimentally demonstrated InGaAs TPV cells in combination with an optimized 2D Ta PhC selective emitter and an optimized cold side tandem filter. This system exhibits $\eta_{\text{TPV}} = 25\%$ and $J_{\text{elec,max}} = 0.68 \text{ W cm}^{-2}$ at realistic $T = 1320 \text{ K}$ and $F = 0.99$. η_{TPV} for this configuration is $\sim 55\%$ of the ideal TPV cell limit shown in Table 1. If TPV cells are to follow a similar research path witnessed by silicon PV cells (reaching $\sim 85\%$ of their theoretical thermodynamic limit), η_{TPV} for this system could reach $\sim 40\%$. Note that the theoretical 0.62 eV single bandgap TPV thermodynamic efficiency limit (with ideal TPV cell and ideal spectral control, which is analogous to the Shockley-Queisser limit for silicon PV), and the theoretical infinite bandgaps TPV thermodynamic efficiency limit (i.e. the Carnot efficiency limit) are respectively 55% and 77% at $T = 1320 \text{ K}$ and $T_c = 300 \text{ K}$.

3.5. Comparisons with notable TPV experimental efforts

To the best of our knowledge, the highest radiant heat-to-electricity efficiency reported to date is 23.6% with $J_{\text{elec,max}} = 0.79 \text{ W cm}^{-2}$ at $T = 1312 \text{ K}$ using InGaAs cells attached with a similar cold side bandpass filter described in Section 2.3, and a greybody-like SiC emitter [43]. Note, however, that this measurement does not include optical cavity losses. If optical cavity losses are included, our numerical model predicts $\eta_{\text{TPV}} = 19.9\%$ and $J_{\text{elec,max}} = 0.80 \text{ W cm}^{-2}$, which is in good agreement with the reported results. A similar experiment, albeit with modifications to include optical cavity losses, and using a greybody-like graphite emitter instead, resulted with $\eta_{\text{TPV}} = 19.1\%$ and $J_{\text{elec,max}} = 0.66 \text{ W cm}^{-2}$ at $T = 1350 \text{ K}$ [44]. Our numerical model, which does not include cell array losses, predicts $\eta_{\text{TPV}} = 20.4\%$ and $J_{\text{elec,max}} = 0.73 \text{ W cm}^{-2}$. If the greybody-like graphite emitter is substituted with an optimized 2D Ta PhC, the TPV system can achieve $\eta_{\text{TPV}} = 20.6\%$ and $J_{\text{elec,max}} = 0.76 \text{ W cm}^{-2}$. Due to the marginal improvements, a greybody-like emitter would be a better choice in a high F system if an optimized tandem filter is present. This result also highlights the need for developing selective emitters that approach the ideal cutoff emitter, possess ultra low ϵ_{lw} , and maintain selectivity over all angles, in order to maintain its relevance in advancing the performance of TPV systems.

For GaSb based TPV systems, the highest radiant heat-to-electricity efficiency reported to date is 21.5% (does not include optical cavity losses) with $J_{\text{elec,max}} = 1.50 \text{ W cm}^{-2}$ at $T = 1548 \text{ K}$ using an anti-reflection coated tungsten emitter with a dielectric filter that transmits useful photons with wavelengths below $1.8 \mu\text{m}$ while reflecting over 95% the photons in the wavelength range $1.8\text{--}3.5 \mu\text{m}$ [54]. This is consistent with the results presented in Table 1. These results also reveal another interesting aspect; spectral control is a great equalizer between different TPV cell technologies. Hence, the simpler, cheaper, and more robust GaSb cells might be the future way forward for practical TPV systems.

4. Conclusion

Spectral control via selective emitters and/or cold side filters is vital towards achieving higher TPV efficiencies. Amongst experimentally demonstrated selective emitters, 2D Ta PhC's hold great promise due to ease of design, large area fabrication, system integration, and ability to withstand extended operation at high temperatures. Most importantly, the selectivity enables up to 100% improvement over a greybody emitter. Substantial improvements in performance can be achieved if further selective emitter development that reduces both long wavelength emittance and angular dispersion is undertaken.

The optimum spectral control approach depends on the achievable view factor, F . For $F > 0.97$ ($10 \text{ cm} \times 10 \text{ cm}$ flat plate geometry with separation $s < 1.7 \text{ mm}$), the greybody emitter outperforms the 2D Ta PhC emitter when coupled with an optimized cold side tandem filter. This is due to high photon recycling efficiency at large F . However, as $F < 0.97$, use of both

the selective emitter and the cold side filter becomes necessary for maximum TPV efficiencies.

By combining an optimized 2D Ta PhC selective emitter with an optimized cold side tandem filter, a TPV energy conversion system with radiant heat-to-electricity efficiency of 25% and power density of 0.68 W cm^{-2} can be achieved using experimentally demonstrated InGaAs TPV cells at realistic emitter temperatures of 1320 K and $F = 0.99$ (10 cm \times 10 cm flat plate geometry with $s = 500 \mu\text{m}$). The efficiency could be increased to $\sim 40\%$ (the theoretical 0.62 eV single bandgap TPV and infinite bandgaps TPV thermodynamic limit at emitter temperature of 1320 K and cell temperature of 300 K are 55% and 77% respectively) if TPV cells are to follow a similar research path witnessed by silicon PV cells, thus paving the way towards widespread adoption of what may be a promising highly efficient, portable, and reliable energy conversion system.

Acknowledgments

The authors would like to thank Peter Bermel and Michael Ghebrebrhan for valuable discussions. We would also like to thank Christine Wang of Lincoln Laboratory for providing us with the InGaAsSb TPV cells in this work. This work was partially supported by the Army Research Office through the Institute for Soldier Nanotechnologies under Contract No. W911NF-13-D-0001. Y. X. Y., W. R. C., and M. S. were partially supported by the MIT S3TEC Energy Research Frontier Center of the Department of Energy under Grant No. DE-SC0001299. V. R. gratefully acknowledges funding by the Austrian Science Fund (FWF): J3161-N20.